CLM-P115

United Kingdom Atomic Energy Authority

RESEARCH GROUP

Preprint

THE ACCUMULATION OF ENERGETIC IONS IN A MIRROR MACHINE BY RESONANT NON-ADIABATIC TRAPPING

A. E. ROBSON
K. L. AITKEN
D. A. ALDCROFT
O. LLOYD
A. H. MORTON

Culham Laboratory,

Culham, Abingdon, Berkshire

1966

UNCLASSIFIED
(Approved for publication)

CLM - P 115

THE ACCUMULATION OF ENERGETIC IONS IN A MIRROR MACHINE BY RESONANT NON-ADIABATIC TRAPPING

by

A.E. ROBSON
K.L. AITKEN
D.A. ALDCROFT
O. LLOYD*
A.H. MORTON/

(Submitted for publication in J. Nucl. Energy Pt C)

* Now at : C.E.G.B., Marchwood Laboratory, Nr. Southampton

/ Now at : Dept. of Engineering Physics, Australian National University, Canberra, Australia.

U.K.A.E.A. Research Group,
Culham Laboratory,
Nr. Abingdon,
Berks.

August 1966 (ED)

CONTENTS

1. INTRODUCTION

The containment of particles in a mirror machine, or adiabatic trap, is generally based on the conservation of the magnetic moment of a particle's gyro-orbit. If the magnetic moment is not rigorously conserved the magnetic mirrors no longer act as impassable barriers to the particles: while this reduces the effectiveness of containment it also allows the trapping of particles injected through the mirrors from an outside source. Such a system is known as a non-adiabatic trap. The injection and temporary capture of a beam in such a trap can lead to an accumulation of particles at a density substantially greater than the density in the beam and limited, in principle, only by the dictates of Liouville's theorem. Thus the trap is of interest at least as the first stage in the creation of a high-temperature plasma from an energetic beam of ions.

Although any method of changing the magnetic moment in a single transit can be used as a capture mechanism, we shall be concerned here almost entirely with the method originally suggested by FEDORCHENKO et al. (1959). Here a beam of particles is injected into a static magnetic mirror trap along the lines of force: the central field of the trap has a small spatially periodic variation of wavelength λ and the velocity of injection v is arranged to satisfy the condition

$$v \approx \frac{\lambda}{2\pi} \cdot \omega_c \qquad \ldots (1)$$

where $\omega_c = eB_o/mc$ is the cyclotron frequency of a particle in the central field B_o. There is then a strong resonant interaction between the particle's orbital motion and its motion through the corrugated field, which can convert a large fraction (typically ~ 50%) of the energy of the particle into motion transverse to the field; the magnetic moment thus acquired causes the particle to be reflected by the end mirror. The subsequent history of a particle is determined by the successive encounters it makes with the modulated central field, which eventually reduces the magnetic moment sufficiently to allow escape through one of the mirrors. In particular the occurrence of the inverse resonance is a strong source of particle loss. On average, however, a particle makes an appreciable number of transits of the system before it escapes.

The capture of electrons in a non-adiabatic trap was first demonstrated by SINELNIKOV et al. (1960a,b) who measured the accumulated space-charge, but did not measure the lifetime of particles in the trap. Numerical calculations of particle orbits were carried out by LAING and ROBSON (1961) and DUNNETT et al. (1965) which gave mean containment times corresponding to 20-80 transits. Containment times of this order were measured in electron experiments by DREICER et al. (1962) and DEMIRKHANOV et al. (1964) using in this case a helical perturbation of the central field as suggested by WINGERSON (1961).

It was suggested by Laing and Robson that the accumulation in a resonant trap could be enhanced by injecting molecular ions, some of which would be dissociated into atomic ions inside the trap by collisions with the residual gas atoms. The atomic ions should be contained for longer than their parent molecules both because they are out of resonance with the field modulations and also because their smaller orbit size favours 'more adiabatic' behaviour. If sufficient particle density were accumulated by external injection for significant dissociation to occur on the trapped protons, exponential build-up of proton density could take place (SIMON, 1960). A resonant non-adiabatic trap with molecular ion injection is thus similar in principle to other molecular-ion injection devices, for example, OGRA (GOLOVIN et al. 1961) or DCX2 (BELL et al. 1962). It differs from these experiments in that an internal injector channel is not required since particles are injected through one of the mirrors: this allows injection to be axially symmetrical and reduces the technical problem of gas evolution due to particles striking the injector. Furthermore the non-adiabatic interaction creates a more isotropic velocity distribution than in other injection devices, and this may be useful in reducing instabilities due to anisotropy in velocity-space.

The density of molecular ions that can be obtained by external injection and the density of atomic ions that can be obtained by dissociation depend in the first place on the lifetimes of the individual particles due to their interaction with the field configuration. This paper is concerned mainly with experiments on the single-particle behaviour of molecular and atomic ions in a resonant non-adiabatic trap, and the interpretation of the results in the light of a theoretical model.

2. RESONANT TRAPPING

Let us consider the central field of the trap to be described by a vector potential $\underline{A}$ which, on account of the axial symmetry, has only an azimuthal component

$$A_\theta = B_{zo} \left(\tfrac{1}{2}r + h\, I_1(kr) \sin kz\right) \qquad \ldots (2)$$

the field components are thus:

$$B_z = B_{zo} \left(1 + h\, I_o\, (kr) \sin kz\right)$$

$$B_r = - B_{zo}\, h\, I_1\, (kr) \cos kz \qquad \ldots (3)$$

where B_{zo} is the unperturbed axial field, $k = 2\pi/\lambda$, I_o and I_1 are Bessel functions and $h \ll 1$.

A particle moving in this field parallel to the axis at radius r_o with velocity $v = v_z$ will experience a periodic transverse force given by

$$F = F_o \cos k\, v_z\, t \quad , \quad F_o = m\, \omega_c\, v_z\, h\, I_1\, (kr_o) \qquad \ldots (4)$$

Under resonance conditions, with $kv_z = \omega_c$, the particle will acquire transverse velocity $v_\perp$ at an average rate

$$\dot{v}_\perp = \tfrac{1}{2} \frac{F_o}{m} = \tfrac{1}{2}\, v_z\, \omega_c\, h\, I_1\, (kr_o) \qquad \ldots (5)$$

So that after traversing n periods of the modulated field, the ratio of transverse energy to total energy will be

$$\xi = v_\perp^2/v^2 = (\pi\, n\, h\, I_1\, (kr_o))^2 \qquad \ldots (6)$$

This relation holds strictly only for $v_\perp \ll v$: as $v_\perp$ increases, the conservation of energy requires the axial velocity v_z to decrease, and this in turn affects the resonance condition, while the variation in B over the finite orbit of the particle needs to be considered. However even when ξ is not small (6) is adequate to describe the magnitude of the resonant transfer of energy from longitudinal to transverse motion. We may regard ξ as a normalised magnetic moment, since this quantity measured in the central field of the trap determined whether

or not a particle will be reflected by a mirror of mirror ratio R through the condition

$$\xi > \frac{1}{R} \qquad \text{(reflection)} \qquad \ldots (7)$$

Provided (7) is satisfied on the first transit, a particle will be captured and its history can then be determined in principle by solving its equation of motion in the field (2) and in the field of the mirrors. However this involves tedious step-by-step numerical integration and the accumulation of errors makes it impracticable to follow a particle for more than about 30 transits. A major simplification was introduced by Dunnett et al. who replaced the field (2) by a 'square wave' field of the same wavelength

$$B = B_{zo} \ (1 \pm h) \qquad \ldots (8)$$

Particle orbits in this field may be calculated algebraically, and accurately followed for long periods. It was shown that for particles satisfying (1) the changes in ξ produced by a single transit through a square-wave field were closely similar to the effect of a sinusoidal field, if a suitable adjustment was made to the modulation amplitude. In particular, for $kr_o \ll 1$, orbits in the two systems could be matched by making

$$h_{\text{square wave}} = \frac{\pi}{4} \ h_{\text{sine wave}} \qquad \ldots (9)$$

By taking large numbers of particles and calculating their orbits over many transits in this model, a statistical picture of containment was obtained, and the dependence of the mean containment time T on the various trap parameters was investigated. For a given number of modulations n, T is optimised when ξ on the first transit is ~ 0.4, which through (6) determines the product $nh\, I_1 (kr_o)$.

Since each particle has a constant of its motion in the canonical angular momentum

$$p_\theta = mrv_\theta + \frac{e}{c} r A_\theta = \frac{e}{c} (rA_\theta)_{r=r_o} \qquad \ldots (10)$$

putting $v_\theta = \pm v$ and substituting for A_θ from (2) gives the radial limits of the region accessible to the particles. If the field is uniform (h = 0) the

limits are, simply

$$r = (r_0^2 + \rho^2)^{\frac{1}{2}} \pm \rho \qquad \ldots (11)$$

where $\rho = v/\omega_c$ is the gyro-radius. The containment region is then a hollow cylinder of thickness 2ρ, while if $h > 0$ the boundaries have a sinusoidal perturbation of order h. Clearly as r_0 is reduced, so is the outer limit radius, and hence the size of the trap, but to ensure capture h must be increased and this rapidly leads to practical difficulties in the coils producing the modulation of the field. A compromise figure of $r_0 = 1.75\rho$, which through (1) gives $kr_0 = 1.75$, was therefore chosen for the experimental design.

The choice of n is also a compromise. T increases with n up to $n = 12$, but the resonance is then excessively sharp in v and r_0, so that for the experimental design we chose $n = 7$. It was estimated that, with the anticipated spread of v and r_0 from the ion source, all injected particles would then be given $\xi > 0.25$ and so be trapped with a mirror ratio of 4. From (6), the value of h needed is then about 0.025.

3. EXPERIMENTAL APPARATUS

A general arrangement of the experimental apparatus is shown in Fig.1.

The magnetic mirror trap is produced by a system of coaxial coils giving a maximum central field of 14 kG and maximum mirror fields of 36 kG: the distance between the peaks of the mirror fields is 308 cm. Modulation of the central field is achieved by a set of 14 coils, connected alternately in opposite senses and arranged in two groups of seven with a gap in the centre to allow diagnostic access. The wavelength of the modulation is 20 cm.

The coils are of water-cooled copper and are energised by batteries of lead-acid cells with a total power of 4 MW. The current in each of the four main circuits is controlled by the arrangement shown in Fig.2: the resistors provide coarse control and the series generator provides fine control and stabilisation through an electronic servo system. The majority of the power is provided by the

battery; the maximum contribution from the generator is 10%. The stabiliser increases the voltage of the generator as the battery voltage falls under discharge and keeps the current in each circuit constant to within 5 parts in 10^4 over a 10 second 'on' period. The battery is charged in the interval between each 'on' period; this takes 5-10 minutes according to the level of operation.

The arrangement of coils round the ion source enables the source to operate in a region of uniform field whose strength is in constant ratio to the field at the centre of the trap, although the mirror ratio may be varied from 2 to 5. Thus the beam diameter as it enters the modulations always has the same value (11 cm), independent of the mirror ratio. The mirror ratio used in the majority of the experiments was 4.

The vacuum system consists of a central tube 22 cm inside diameter and 370 cm long, having diagnostic access ports in the middle and a large pumping manifold at each end. Each manifold has two 14 inch oil diffusion pumps and provision for titanium evaporation. The construction is of stainless steel with gold-wire gaskets and is designed for baking to 450°C. A base pressure of 2.10^{-9} torr can be obtained.

The injector is connected to the trap by means of a long annular channel through which the ions are guided by the magnetic field; various collimators can be fitted in the channel to restrict the flow of gas from the ion source, but in operation the pressure of hydrogen in the machine is always at least one order of magnitude greater than the base pressure.

The ion source is a hot-cathode reflex arc burning in an annular slot in a water-cooled anode. The ions are extracted from the end opposite to the cathode, the ion extraction potential acting as the reflector of the arc electrons. The source will give currents in excess of 100 mA of H_2^+ ions in an annular beam at energies up to 35 keV. The H_2^+ ions are usually accompanied by a few per cent of H_1^+ and about 15% H_3^+ ions. The accelerating voltage is stabilised to 1 part in 10^4, using a series triode. The arc can be switched off by a circuit employing silicon controlled rectifiers, one of which is used to short circuit the arc. The ion beam then decays with a time constant of $\sim$ 2 μsec.

4. DETAILED STUDY OF THE TRAPPING PROCESS

The modulation produced by the finite set of lumped coils shown in Fig.1 is somewhat different from the simple expression (2). The measured variation of B_z on the axis of the experiment is shown in Fig.3 for the case when the current in the modulation circuit (I_{mod}) is equal to the current in the main circuit (I_{main}). Also shown is a square-wave model of this field, which has been constructed by placing the field steps at the positions of maximum dB_z/dz of the real field, and taking the amplitudes of the square-wave proportional to the measured peak amplitudes. Since the amplitudes are not equal, h now denotes a mean amplitude and suitable weighting factors are applied to the individual modulations. The square-wave model must be matched to the real system through a proportionality factor Υ given by

$$h = \Upsilon I_{mod}/I_{main} \quad . \qquad \ldots (12)$$

Following Dunnett et al. we calculate the orbits of particles through the square-wave model for a large number of values of h and initial velocity v. All particles start with $\xi = 0$ at $kr_o = 1.75$. Contours of ξ after one transit are plotted in Fig.4 as functions of h and v, values of v being normalised to the resonant velocity ω/k. The main resonance is seen clearly as a hill with peak occurring at $v \approx 1.1$, a slightly greater velocity than given by the simple resonance condition because of the loss of axial velocity as the particle gains transverse velocity.

For a particular value of $I_{mod}/I_{main} = 1.125$ a series of particle orbits in the experimental field were obtained by numerical integration of the equations of motion. The modulation was taken as due to fourteen current loops placed at the centres of the modulating coils. A curve of ξ against v obtained from these calculations is shown in Fig.5 (curve 1). A section through Fig.4 at $h = 0.036$ gave curve 2. The two curves have the same height and closely similar shape: the correspondence of the peak amplitudes is expressed by putting $\Upsilon = 0.032$ in equation (12). The h-axis of Fig.4 can now be calibrated in terms of I_{mod}/I main

and the figure then gives a complete description of the initial capture process in the experimental trap.

Using equation (10) with $v_\theta = v$ and (rA_θ) as calculated for the field system of the experiment, we obtain a boundary in (h, v) shown in Fig.4, beyond which the outer limit radius intersects the vacuum wall. The input conditions must therefore be chosen to lie below this boundary.

The orbits of ions on their first transit were studied experimentally with the aid of a fluorescent screen which could be moved on a railway down the entire length of the apparatus. For this purpose the ion source was blanked off except for one small circular hole, to give a point source of ions. Fig.6 shows the patterns observed on the screen at different axial positions, for the conditions listed in the caption. The pictures are as follows:

(a) Screen 95 cm from midplane, no modulation.

(b) As (i) but with modulation coils switched on. There are three separate traces, corresponding to the three ion species H_1^+, H_2^+ and H_3^+. The H_1^+ are virtually unaffected by the modulations. The H_2^+ and H_3^+ traces are of comparable radius: they may be distinguished by measuring the rate of rotation of the pattern as the screen is withdrawn. Although the H_3^+ has the slightly larger radius, the transverse energy is in fact less than the transverse energy of the H_2^+.

(c) Screen withdrawn to 125 cm from midplane. The traces become complete circles and contract in diameter, illustrating the property of the magnetic mirror of spreading the phase of the particles in their gyro-orbit while conserving the magnetic moment. The transverse energy can be calculated from the diameter of the orbits, since the field is known. Referring back to the central field we derive that $\xi = 0.35$ for H_2^+ and $\xi = 0.24$ for H_3^+.

(d) Screen withdrawn to 135 cm from midplane. This is beyond the reflection point for H_2^+ ions, which are captured in the trap and emerge after successive reflections as a band on the screen, spread out in the direction in which the orbits precess due to the field curvature in the mirrors. This pattern persists as the screen is withdrawn through the throat of the mirror. The H_3^+ ions are not reflected, due to their smaller ξ, and pass straight through the system (mirror ratio 4).

These pictures provide a good qualitative description of the first transit of the ion beam. The transverse energy acquired by the H_3^+ can be understood in terms of Fig.5: resonant H_2^+ ions with $v \approx 1.1$ will be accompanied by H_3^+ whose momentum is equivalent to H_2^+ having $v \approx 1.35$ which lie on the second, smaller resonance. Quantitatively, ξ for the H_2^+ ions is as expected from Fig.4, but ξ for the H_3^+ is somewhat larger.

To investigate the resonances more accurately, further experiments were performed using an electron gun in place of the ion source; the electron energy was ~ 30 keV and the magnetic fields were reduced so that the system scaled to resonate with the electrons. The electron experiments removed the confusion of the several ion species and the lower fields allowed the apparatus to be run continuously instead of in 10-second pulses. It was found that the variation of ξ with v, keeping h constant, followed the general shape predicted by the computations, but that a fine-structure of hills and valleys was superimposed; this variation is shown dotted in Fig.5.

We attribute the fine-structure to the slight non-adiabaticity of the orbit in the mirror through which the particles are injected. Although launched accurately along the field ($\xi = 0$) they arrive at the modulations with $\xi = \xi_0$ which can either augment or decrease the ξ produced by the modulations according to the phase φ_0 at which the particles reach the first modulation. From analogue computations by READ (1965), it is estimated that $\xi_0 \simeq 0.01$. Assuming particles leave the ion source with $\varphi = 0$, they reach the modulations with

$$\varphi_0 = \int \omega dt = \frac{e}{mcv} \int B \, dz \qquad \ldots (13)$$

which at the resonant velocity becomes

$$\varphi_0 = k \int \frac{B}{B_0} \, dz \qquad \ldots (14)$$

Taking the integral over the measured field gives $\varphi_0 = 28.5\pi$, and since

$$\frac{\Delta\varphi_0}{\varphi_0} = - \frac{\Delta v}{v} \qquad \ldots (15)$$

a phase change of π will occur for $\Delta v/v = 0.035$, which corresponds to the separation of the peaks in Fig.5. The magnitude of the peaks can be accounted for by taking $\xi \simeq 0.01$. This phenomenon has an effect on containment which will be discussed later.

The secondary peak at $v \approx 1.25$ is found to be somewhat larger than predicted, possibly also because of finite ξ_0. The phasing appears to be less important here since no fine-structure is seen. Since $\xi_{max} > 0.25$ it is possible to trap particles by tuning to this peak, but as can be seen from Fig.4 the outer limit surface will then intersect the vacuum wall and so the peak is not useful for long-term containment.

5. CONTAINMENT EXPERIMENTS USING ELECTRONS

With a point source of electrons and the conditions set for resonant capture, the pattern observed on a fluorescent screen placed outside the end mirror is shown in Fig.7. The source is at the top of the picture and the trapped particles precess clockwise about the axis at a calculated average rate of about 2^o per transit: thus the azimuth at which a particle emerges from the trap is an approximate measure of its containment time. The features revealed by this picture are as follows:

(a) The distribution of brightness indicates that there are heavy losses occurring in the first 10 transits but that there is a long tail of contained particles having lifetimes of up to at least 180 transits.

(b) The fine-structure of the pattern in the neighbourhood of the injection point shows that the beam retains some of its discreteness for a few transits, but thereafter electrons emerge with a continuous distribution in velocity space within the loss cone.

(c) The concentric bands in the pattern, which persist throughout the tail, indicate that there are preferred values of ξ in the distribution of emerging particles. The bright band on the injection radius is due to particles emerging with $0 \leqslant \xi \leqslant 0.005$, corresponding to loss by the inverse of the resonant capture process. The pair of bands on either side of the injection radius is due to particles emerging with $\varepsilon \simeq 0.05$.

(d) The sharp edges to the containment pattern are a confirmation of the limit surfaces predicted by equation (11).

6. CONTAINMENT OF IONS

To determine the rate of precession about the axis, ion injection was used and a segment of the end target was placed so as to receive particles which had precessed between 180^{o} and 270^{o} from the injection azimuth. A pair of ring electrodes in front of the segment were biased to -300 V with respect to earth to repel electrons from the trap and suppress secondary emission from the segment. The current to the segment as a function of time after the H_2^+ beam is turned <u>on</u> is shown in Fig.8 (which also shows the location of the segment with respect to the containment pattern of Fig.7). The current begins to rise after 300 μsec and reaches a steady state value after 800 μsec, from which we deduce that the precession frequencies of the particles lie in the range 1-1.7 kc/s. A second rise in current then occurs due to the arrival of slow ions, which have been formed by ionizing and charge exchange collisions in the trap. From the displacement between the first and second current rises, their lifetime τ_s can be estimated as approximately 800 μsec, which is consistent with their moving out along the field at thermal speed. The fast and slow ion currents are of comparable magnitude in this case ($p \sim 10^{-7}$torr).

The mean containment time τ is given by

$$\tau = \frac{\int_0^\infty t.\, i(t)\, dt}{\int_0^\infty i\,(t)\, dt} \qquad \ldots (16)$$

where $i(t)$ is the total escaping ion current at time t after cut-off. Since the decay is not necessarily exponential, $i(t)$ must be measured over all t and in particular the tail of the decay makes an important contribution to τ. The tail is easily masked by slow plasma effects which tend to neutralise the fast ion space-charge, and so estimates of τ based on measurements of current decay from the ends were not considered reliable.

An unambiguous method of measuring fast ion containment is to measure the flux to the wall of fast neutral atoms formed by charge exchange and dissociating collisions between the contained ions and the background gas. If the ions are contained

in a long cylindrical region of radius r_1 within which their mean density is n_2 and the density of neutral gas atoms is n_0, the flux F of fast neutrals to a detector at radius r_2 is given by

$$F = n_0 n_2 v \frac{r_1^2}{2r_2} (\sigma_1 + 2\sigma_3) \quad \text{equivalent protons/sec} \quad \ldots (17)$$

where the cross-sections are defined in Table I.

TABLE I

COLLISION CROSS-SECTIONS IN H_2 GAS

Production of fast H_1^0 by 16 keV H_2^+	$\sigma_1 = 8.0 \cdot 10^{-16}$ cm^2/molecule*
Production of fast H_1^+ by 16 keV H_2^+	$\sigma_2 = 2.0 \cdot 10^{-16}$ cm^2/molecule*
Production of fast H_2^0 by 16 keV H_2^+	$\sigma_3 = 4.0 \cdot 10^{-16}$ cm^2/molecule*
Production of fast H_1^0 by 8 keV H_1^+	$\sigma_4 = 8.0 \cdot 10^{-16}$ cm^2/molecule*
Production of slow H_2^+ by 16 keV H_2^+	$\sigma_5 = 7.0 \cdot 10^{-16}$ cm^2/molecule†
* McCLURE, 1963	† AFROSIMOV et al., 1958

The mean containment time τ is

$$\tau = \frac{n_2 V}{I} \quad \ldots (18)$$

where I is the injection current and V the volume of the trap, and when normalised to unit transit time $\tau_0 = L/v$, where L is the length of the trap, becomes

$$T = \frac{n_2 \pi r_1^2 v}{I} = \frac{2\pi r_2 F}{n_0 I(\sigma_1 + 2\sigma_3)} \quad \text{(equivalent transits)} \quad \ldots (19)$$

Thus T is the factor by which the line density of ions in the central region of the trap is increased over the line density of ions in the beam, and is a measure of the effectiveness of the trap as an accumulator of particles. The mean number of mirror reflections is about T/2. The effective length L which must be used to derive T from τ is 250 cm, so for 16 keV H_2^+, $\tau_0 = 2$ μsec.

Using equation (19), T can be derived from measurements of n_o, F and I. The density of neutral atoms, n_o, was measured during the operating period by means of a novel ionization gauge situated in the diagnostic block and capable of operation in the main magnetic field of the machine. This gauge, working on the principle of virtual cathode neutralisation, is described fully elsewhere (LLOYD, 1966).

The flux F was measured by scintillation detectors in the midplane of the machine. Each detector consisted of a $C_sI(Tl)$ crystal with an exposed area of 1.6 cm^2 connected by a perspex light guide to a photomultiplier, the latter being outside the main coil system of the machine and shielded against stray magnetic fields. A shield on the crystal ensured that the detector received particles only from the half of the machine away from the injector: this was to eliminate spurious signals from fast neutrals and light from the ion source.

The detectors were calibrated in a separate apparatus with beams of H_2^+ and H_1^+ ions of 5-50 keV, and it was assumed that the calibration would be unaltered for neutral particles of the same mass and energy.

Since equation (17) assumes a cylindrically symmetrical system all measurements were made with an annular ion beam, collimated on entry by a ring of cylindrical holes (collimator 1, Table II). The azimuthal distribution of injected current was checked by a segmented target inserted in path of the beam for this purpose. It was usual to use two detectors separated in azimuth by 90^o whose outputs were measured separately and then combined. It is estimated that the error in measuring mean density arising from imperfect azimuthal distribution of fast ions did not exceed 10%.

TABLE II

Collimator 1	18 holes, 2 mm dia., 10 mm long	I_{max} = 2 mA p = $5.0 \cdot 10^{-7}$ torr
Collimator 2	57 holes, 4 mm dia., 10 mm long	I_{max} = 12 mA p = $1.5 \cdot 10^{-6}$ torr
Collimator 3	Slit 23 mm wide, 175 mm long	I_{max} = 40 mA p = $2.0 \cdot 10^{-6}$ torr

By applying the scintillator output to the vertical amplifier and a voltage proportional to the injection energy to the horizontal amplifier of an oscilloscope, the resonance curve could be traced by sweeping the H.T. supply. Fig.9 shows a typical curve, together with the current received at the end target of the machine. The oscillatory structure within the resonance is attributed to the effect of finite initial ξ, as discussed in Section 4. At resonance, the end current drops to approximately half its untrapped value, and an approximately equal current emerges from the injector end of the machine.

As will be shown later, the contribution to the scintillator signal from trapped H_1^+ ions cannot under these conditions exceed 12% and is probably no more than 6%: correcting the signal by the latter figure and using equation (19) the optimum containment (corresponding to the peak neutral flux at E = 16.4 kV) is $T = 29 \pm 9$ transits.

A more direct measurement of mean containment time is obtained by observing the decay of fast neutral flux after the ion beam has been turned off. The decay curve taken for conditions corresponding to the peak of Fig.9 is shown in Fig.10(a) and a similar curve close to the first minimum in Fig.10(b). Provided the beam has been injected for long enough that a steady state has been established, the mean containment time τ is given by the intercept on the time axis of the tangent to the decay curve at cut-off. This method is independent of the absolute calibration of the detector, and can be applied to non-exponential decay curves as it does not require detailed knowledge of the shape of the curve. In practice uncertainties are introduced by the step-like nature of the curve immediately after cut-off, which is due to resolution of individual transits, and from Fig.10(a) we can only derive $\tau = 60$–90 μsec, corresponding to $T = 30$–45 transits.

The step effect may however be exploited to derive T, since the first step δ is the contribution to the signal of the entire injected beam as it passes the detector after its first reflection by the end mirror. Hence

$$T = \frac{2F}{\delta} (1 - \xi_1)^{-\frac{1}{2}} \quad \text{transits} \qquad \ldots (20)$$

where the factor 2 arises because the shielded detector only receives neutrals from ions making transits in the reverse direction, and the factor $(1 - \xi_1)^{-\frac{1}{2}}$ arises because the step δ is produced by particles whose axial velocity is less than their total velocity by this factor. Taking ξ_1 as 0.4, from Fig.10(a) and equation (20) we derive $T_{opt} = 35 \pm 3$ transits. This therefore represents the most accurate method of determining T, and was used to confirm that the lifetimes for the conditions at the minima of Fig.9 were about half the corresponding values at the maxima (from Fig.10(b), $T = 16 \pm 2$ transits).

Reducing h leads to a reduction in the spikiness of the resonance and a reduction in T_{opt}; increasing h up to the maximum (0.04) set by the radial containment limit results in no significant increase in containment, so $T = 35$ transits represents the optimum to which the trap can be tuned.

The measured values of T include loss by dissociation and charge exchange, for which the lifetime t_2 is given by

$$1/t_2 = n_o \, (\tfrac{1}{2}\sigma_1 + \tfrac{1}{2}\sigma_2 + \sigma_3) \, v \qquad \ldots (21)$$

where the cross-sections are defined in Table I. For the conditions of Figs.9 and 10, $t_2 = 500$ μsec ($T_2 = 250$ transits). The non-adiabatic lifetime T_{NA} is then given by

$$\frac{1}{T_{NA}} = \frac{1}{T_{measured}} - \frac{1}{T_2} \qquad \ldots (22)$$

so the optimum value of T_{NA} is 40 transits.

7. CONTAINMENT OF DISSOCIATED PROTONS

With the standard magnetic field setting, the optimum containment of H_2^+ occurred at an injection energy of 16.4 keV. Since the orbit of a particle in the machine is determined only by its momentum, H_1^+ ions of 32.8 keV and H_3^+ ions of 10.9 keV have containment histories identical to 16.4 keV H_2^+ if the respective time scales are normalised to unit transit time. By sweeping the injection energy over a wide range while monitoring the neutral flux, the trap

could be used as a mass spectrometer: in this way the output from the ion source was found to consist of 80% H_2^+, 15% H_3^+ and 5% H_1^+.

Neutral flux decay curves obtained for alternate injection of 32.8 keV H_1^+ and 16.4 keV H_2^+ are shown in Fig.11, with the timebase for H_1^+ twice as fast as for H_2^+. As might be expected, these curves are closely similar, but the H_2^+ decay contains a component due to charge exchange of 8.2 keV H_1^+ formed by dissociation inside the trap. This is particularly apparent in the long tail ($t > 200$ transits) after the curves have been corrected for charge exchange. The tail was recorded simultaneously on a second oscilloscope at ten times the amplification. Reproducibility of the curves from shot to shot was within 8%, and after conversion to digital form the curves were averaged in groups of four. A correction was then made for the effect of scintillator afterglow, which was determined from a separate experiment. The H_1^+ decay curve $F_1(t)$ was then corrected for charge exchange:

$$F(t) = F_1(t)\, e^{t/t_1} \qquad \ldots (23)$$

where $t_1 = 1600$ μsec is the charge exchange time for 32.8 keV protons in the ambient gas pressure of $2 \cdot 10^{-7}$ torr. $F(t)$ is now the decay curve for injected particles arising solely from their non-adiabatic interaction with the magnetic field, and should be applicable to injected molecular ions provided t is suitably normalised to unit transit time.

The decay curve for H_2^+ injection should then be given by

$$F_2(t) = (1 - \alpha)\, F(t)\, e^{-t/t_2} + \alpha\, e^{-t/t_3} \qquad \ldots (24)$$

where t_2 is defined by (21) and is in this case 1200 μsec, and α is the fraction of the steady-state neutral signal due to the dissociated (8.2 keV) protons assumed to have an exponential decay with mean lifetime t_3. As the protons may be lost by both charge exchange collisions and non-adiabatic effects we have:

$$\frac{1}{t_3} = n_0\, \sigma_4\, v + \frac{1}{t_p} \qquad \ldots (25)$$

where t_p is the lifetime of the 8.2 keV protons due to the non-adiabatic effects alone.

The ratio of the proton density n_1 and the molecular ion density n_2 in the steady-state is

$$\frac{n_1}{n_2} = \frac{\sigma_2}{\sigma_4 + 1/n_0 v t_p} \qquad \ldots (26)$$

from which we may derive

$$\alpha = \frac{n_1 \sigma_4}{n_1\sigma_4 + n_2(\sigma_2 + 2\sigma_3)} = (1 + (1 + 2\sigma_3/\sigma_2)(1 + 1/n_0\sigma_4 v t_p))^{-1} \qquad \ldots (27)$$

Using the experimentally determined function $F_1(t)$ and equations (23) to (27) we may construct curves of $F_2(t)$ for different values of t_p.

In Fig.12 are shown the relevant portions of F_2 computed for $t_p = 0$ ($\alpha = 0$) and $t_p = \infty$ ($\alpha = 0.12$). The experimental H_2^+ decay is also shown, for which the best fit to a computed curve is obtained when $t_p = 1400$ μsec ($\alpha \approx 0.06$). Protons formed in the trap are thus subject to non-adiabatic loss corresponding to a lifetime of ~ 700 transits, but in view of the many different factors involved the accuracy of this figure is probably no better than ± 200 transits.

8. HIGH CURRENT INJECTION

For the measurements described so far the ion source was usually set to give a total current of 50 mA, which was reduced to ~ 2 mA by collimator 1 between the injector and the trap. Two other collimators with larger apertures were available which allowed a greater proportion of the current to be injected, but at the expense of increased ambient pressure in the trap due to neutral gas flowing from the injector (see Table II).

With continuous high-current (~ 50 mA) injection there was a serious increase in the neutral pressure due to bombardment of the ends by escaping ions and bombardment of the walls by fast neutrals: even after the system had been baked at 200°C for several hours 5-10 neutral atoms were released per incident fast particle. However, by injecting the beam in pulses of 5 msec duration, repeated once a second, the pressure rise during injection was restricted to less than 10% of the ambient values in Table II.

Within the range of a given collimator, the ion current was adjusted by varying the arc current in the ion source. The fast ion density in the trap was then measured by the methods described in Section 6. The dependence of density on injected current is shown in Fig.13. For a given collimator the dependence is linear, but the mean lifetime T, given by the slope of the line, varies according to the collimator used. The difference in T between collimators 2 and 3 can be accounted for by the increased charge exchange loss with collimator 3: the non-adiabatic lifetime is the same in each case (18 transits) within the limits of error, compared with a non-adiabatic lifetime of 40 transits for collimator 1.

The reduced lifetime observed with the larger collimators is associated with a change in the nature of the resonance curve. The neutral signal obtained by sweeping the injection voltage through resonance, using collimator 2, is shown in Fig.14. This should be compared with Fig.9 which was obtained with collimator 1. With the larger collimator the fine structure has largely disappeared, so that it is no longer possible to obtain maximum containment by fine-tuning to one of the subsidiary peaks on the resonance curve.

9. CONTAINMENT AND THE SQUARE WAVE MODEL

Having selected the initial conditions (h, v) from Fig.4, the state of a particle at any subsequent time can be adequately described by only two quantities, ξ the normalised magnetic moment and φ the phase of the particle in its gyro-orbit. (ξ', φ') after a transit of the modulations is a function of (ξ, φ) at the moment of entry: by calculating a large number of single transits for different initial conditions we derive $\xi'(\xi, \varphi)$, which is presented as a contour map in Fig.15(a). Here $h = 0.037$ and $v = 1.1$, corresponding to the standard experimental conditions. The map is a complete description of the effect of the modulations in changing the ξ of a particle on the first and any subsequent transit.

The mirrors are assumed to reflect particles without changing ξ (provided the reflection condition $\xi > 0.25$ is satisfied) and it is further assumed that

since a particle makes many gyro-revolutions in the mirror field the phase with which it returns to the modulation region is uncorrelated with the phase with which it enters the mirror. The development of the traces on the fluorescent screen (Fig.6) into full circles as the screen is withdrawn shows that all phases are present after reflection and is taken as justifying the assumption of uncorrelated phase.

Accordingly, with the phase change in the mirrors determined by a random number generator, particle orbits are calculated through the system from injection ($\xi = 0$) until eventual loss through one of the mirrors ($\xi < 0.25$). The time spent in the trap is normalised to unit transit time so that the mean lifetime, obtained by averaging over 1000 particles, corresponds to the quantity T measured in the experiments. By calculating T for different values of v the resonance curve of Fig.16 is obtained, with a peak value of $T = 14$ transits and a width $\Delta v/v = 0.06$.

These calculations do not predict the fine-structure of the resonance observed with collimator 1 (Fig.9) which is attributed to the beam acquiring a small magnetic moment ξ_0 on traversing the input mirror. This can increase or decrease the magnetic moment ξ_1' acquired on the first transit, according to the phase φ_0 at which particles arrive at the modulations. In Fig.17 is shown a section of Fig.15(a) at $\xi_0 = 0.01$, giving ξ_1' as a function of φ_0. Also shown are corresponding values of T calculated from 1000-particle containment runs: the larger values of T are associated with larger values of ξ_1'. As discussed in Section 4, φ_0 is sensitive to small changes in v and can be changed by more than 2π within the width of the resonance, leading to three peaks in ξ_1' (Fig.5) and three corresponding peaks in T (Fig.9). In Fig.17 there are positions of no containment between the peaks, whereas Fig.9 shows only minima: due to the extreme sensitivity of containment to input conditions, the small spread in v, p_θ and ξ among particles from the ion source is probably sufficient to ensure containment of some particles at any point within the resonance.

The maximum T from Fig.17 is 30 transits, corresponding to $\xi_1' = 0.45$. To obtain the measured value of $T = 40$ it is necessary to take $\xi_1' = 0.48$: this

illustrates the sensitivity of T to ξ_1', and in view of the uncertainty in our knowledge of the exact spread in initial parameters, the discrepancy between theory and experiment is not serious.

The larger collimators are capable of admitting a beam which starts with a spread in ξ_0 of the same order as the ξ_0 introduced by the non-adiabaticity of the first mirror: φ_0 is then spread over 2π, the phase selectivity is lost, and a resonance curve closely similar to Fig.16 is obtained, but with 50% greater width.

The statistical containment calculations also produce the distribution of particle lifetimes, from which the density decay curves can be constructed. In Fig.18 the characteristic decay curve of the trap, obtained with H_1^+ injection (Fig.11) and corrected for charge exchange, is compared with the curve calculated from the square-wave model for conditions giving the same mean containment ($\xi_1' = 0.48, T = 40$). The agreement is good. Also shown is an exponential with the same mean lifetime, and the theoretical curve of current out of the ends; the latter is the derivative of the density decay curve, and emphasises its non-exponential nature. Current decay curves of similar shape have been observed in electron containment experiments by DREICER et al. (1962) and DEMIRKHANOV et al. (1964).

Losses from the trap occur over a variety of possible exit paths and due to the symmetry of the system and the time-reversal property of the orbits each exit path is also a possible entry path. In Fig.15(a) the shaded region $\xi < 0.25$, $\xi' > 0.25$ defines the range of (ξ, φ) for which an injected particle may be captured, and the probability of capture $P(\xi)$, assuming all phases present, is shown in Fig.15(b). If the system were in equilibrium with injection and loss occurring at equal rates over each path, $P(\xi)$ would also represent the probability that a particle escapes with that value of ξ. The two maxima in $P(\xi)$ at $\xi = 0$ and $\xi \approx 0.1$ indicate that there are preferred ξ-values among the escaping particles (particularly the 'inverse resonance' close to $\xi = 0$), and although the experimental situation does not satisfy the conditions of detailed balancing, preferred ξ-values are observed as bright bands on the fluorescent screen (Fig.7).

10. SQUARE-WAVE MODEL FOR DISSOCIATED PROTONS

The square-wave model appears to be a realistic analogue of a system in which the 'adiabatic parameter' $\varepsilon = 2\pi\rho/\lambda \geqslant 1$, that is to say a highly non-adiabatic system, such as is experienced by the injected particles. The field experienced by the dissociated protons differs in two significant respects: there is no longer resonance between the gyro motion and the field, and also the motion is 'more adiabatic' since now $\varepsilon \approx 0.5$.

For the purpose of calculating proton orbits through a square-wave modulation, the first point can be simulated by considering particles with half the momentum of the parent molecules ($v \simeq 0.5$) while the second can probably be simulated by suitably reducing h. As a first attempt, orbits were calculated for $h = 0.019$ (half the value appropriate for injected particles) and with particles starting inside the trap in groups of 250 at 7 values of ξ from 0.3 - 0.9 to simulate an isotropic source. The mean lifetime T was 109 transits. The calculation was repeated with groups of 100 particles for $h = 0.012$ and gave $T = 250$ transits. To reduce h further would have been inordinately expensive in computer time, but the above results are consistent with $T \propto 1/h^2$, as might be expected for a stochastic process, so by extrapolation the measured value $T \approx 700$ transits would be consistent with taking $h = 0.0075$, a reduction by a factor of 5 on the effective step for molecular ions.

11. OPTIMISATION OF NON-ADIABATIC TRAPS

ROBSON and TAYLOR (1965) have shown that the maximum accumulated density in a non-adiabatic trap is obtained when injection and loss occur at equal rates over all available paths. The trapped particles then fill uniformly all the phase-space available to them, and their distribution in velocity space is such that the number of particles having pitch angles between ψ and $\psi + d\psi$ (where $\psi = \sin^{-1} \xi^{\frac{1}{2}}$) is proportional to $\sin \psi \, d\psi$. The main shortcoming of a resonant trap with injection close to $\xi = 0$ is that only a small fraction of the available paths are used for injection, while all are available for loss. To ensure that all entry

paths were used would, in our experiment, require the beam to fill the entire loss cone at both ends. Assuming all phases present, the fraction of the beam which would be captured is

$$f = \frac{\int_0^{\psi_m} \sin\psi\, P(\psi)\, d\psi}{1 - \cos\psi_m} \qquad \ldots (28)$$

where $P(\psi)$ is the capture probability derived from Fig.15(b) and $\psi_m = \sin^{-1}R^{-\frac{1}{2}}$.

Following Robson and Taylor, the mean lifetime of the captured particles, $\bar{T}$, is derived by balancing rates of injection and loss:

$$\int_0^{\psi_m} \sin\psi\cos\psi\, P(\psi)\, d\psi = \frac{\cos\psi_m}{\bar{T}} \qquad \ldots (29)$$

and using Fig.15 to evaluate the integrals we obtain $f = 0.52$ and $\bar{T} = 14$, so for a beam filling the loss cones, $T \simeq f\,\bar{T} = 7.3$. If particles were injected only over the shaded region of Fig.15(a) we should have $T = \bar{T} = 14$, but from the complicated shape of the acceptance region, this would require a beam defined in phase and exceedingly hard to produce. The phase-selection which occurred fortuitously in our experiments showed that a narrow beam could be injected in some local area of the acceptance region where the containment time is significantly higher than the average. Contours of constant ξ_1' in Fig.15(a) are also contours of constant T, and in general T increases with ξ_1'. However, containment time alone is less important than the product of containment time and beam current, and this is maximised only by utilising all entry paths.

The beam admitted by the larger collimators was broad enough in ξ to cover the whole range of ξ_1', but since it was restricted to $\xi \ll 0.25$, where $P(\xi) \simeq 1$, from the foregoing arguments we expect $T \simeq \bar{T} = 14$. The measured value of T was 18 (Fig.13).

If we assume that our 40 mA beam filled the region $0 \leqslant \xi \leqslant 0.01$, a beam having the same phase space density and filling the entire loss cone would carry a current of $\sim$ 7A. Two such beams (injected one from each end) should then produce a trapped density of $2.5 \cdot 10^9$ ions cm^{-3}.

A more economical way of achieving the maximum trapped density is to devise a trap in which the acceptance region is equal to or smaller than the extent in ξ-space of the given ion beam. This appears somewhat impracticable in a resonant trap but may in principle be achieved in the 'stochastic' trap described by Robson and Taylor where a small, non-resonant field perturbation serves to capture particles injected in a small band $\Delta\xi_b$ close to the edge of the loss cone. The non-adiabaticity of the trap is adjusted by varying the field perturbation until the acceptance band of the trap, $\Delta\xi_t$, matches the size of the beam, $\Delta\xi_b$. This system can be made single-ended by making one mirror stronger than the other. The containment time is then given by

$$T = \frac{4 \cos \psi_m}{\Delta\xi_t} \qquad \ldots (29)$$

Had we re-arranged our apparatus to form a stochastic trap and redesigned the ion source to give a 40 mA beam with $0.24 \leqslant \xi_o \leqslant 0.25$ (which implies the same phase-space density as the beam from the existing source in the range $0 \leqslant \xi_o \leqslant 0.01$ a trapped density of $2.5 \cdot 10^9$ ions cm^{-3} ($T = 340$) should theoretically have been achievable for an injected current of only 40 mA, compared with the 14A necessary in the case of the existing trap. In both cases the maximum density is achieved by ensuring that the phase space density throughout the trap is equal to the phase space density in the beam (the so-called 'Liouville limit'), but the economy of matching the trap to the beam rather than vice versa is strikingly apparent.

12. STABILITY

Plasma in a simple mirror machine configuration is predicted to be unstable to flute unstabilities when the plasma density n exceeds a critical value at which the ion Debye length $\lambda_D = (kT_i/4\pi ne^2)^{\frac{1}{2}}$ satisfies

$$\lambda_D \leqslant (Rr)^{\frac{1}{2}} \qquad \ldots (30)$$

where r is the plasma radius and R is the 'effective radius of curvature' of the field lines (KADOMTSEV, 1961). Since the instability arises from the

differential precession of ions and electrons, it is desirable to express R in terms of the angular precession frequency of the ions Ω, which is a measurable quantity. Thus

$$\Omega = \frac{v^2}{\omega_c R r} \qquad \ldots (31)$$

For our system, $\Omega \approx 10^4$ radians/sec (Section 6) and thus from (30) and (31) $n_{critical} \approx 10^5$ ions cm^{-3}.

In our experiments a density three orders of magnitude greater than this was obtained, and no indication of flute instability was found. An electrostatic probe of area 0.8 cm^2 was placed in the mid-plane of the machine about 1 cm outside the plasma surface. Had flute instability been present, characteristic low frequency signals at $\Omega/2$ would have been seen due to capacitative coupling of the rotating surface charges on the plasma. No such signals were observed and the small amount of noise appearing on the probe ($\sim$ 10 mV r.m.s.) consisted of frequencies of $\sim$ 10 kc/s and corresponded to potential fluctuations on the plasma of only a few volts. The noise appeared to be due to fluctuations on the ion beam. The linear dependence of trapped density on injected current (Fig.13) would seem to confirm the absence of losses other than by non-adiabatic effects and charge exchange.

The absence of instability is noteworthy since the threshold for the onset of flutes given by (30) has been verified to within a factor 5 in the PHOENIX neutral injection mirror machine (KUO et al, 1964). Even this discrepancy can be largely accounted for by the short axial length of the PHOENIX plasma, since the theory assumes a long cylindrical plasma shape. Our plasma has a length/diameter ratio of 15, and so the theory should apply more closely to our case. However, on account of the elongated shape, the precessional frequency Ω is about 100 times lower than in PHOENIX: electric fields arising from ambipolar effects may thus have a greater influence on the precessional motion, and in certain circumstances may lead to stability (see GOLOVIN et al. 1964).

The fact that our plasma is a hollow cylinder only one gyro-orbit thick should not seriously affect the stability criterion. The hollowness is most apparent in

the mirrors (see Fig.7) but in the central region the inner and outer mean radii, given by equation (11), are 1.5 cm and 9.5 cm respectively so the central hole is relatively small. The plasma in OGRA also has a radius of only one molecular gyro-orbit, and this shows flute instability at a density of $\sim 10^6$ cm^{-3}.

The most likely cause of stability is the background cold plasma, which acts as an electrical connection between the trapped hot plasma and the end plates, and short-circuits the electric fields associated with the growth of flutes. The cold plasma density can be estimated by balancing the rates of production and loss of slow ions in the steady state. Thus if n_2, n_s, n_o are the densities of fast molecular ions, slow ions and neutral atoms respectively we have

$$n_o \, n_2 \, \sigma_5 \, v = \frac{n_s}{\tau_s} \qquad \ldots (32)$$

where v is the ion velocity, σ_5 is defined in Table I, and $\tau_s = 800$ μsec from Section 6. Thus

$$\frac{n_s}{n_2} = 2.5 \cdot 10^6 \cdot p \qquad \ldots (33)$$

where p is the neutral pressure in torr. With collimator 1 we therefore have $n_s \approx n_2$ and with collimator 3, $n_s \approx 5n_2$.

There appears to be no comprehensive theory of the stabilising effect of cold plasma which takes into account the exact nature of the connection to the ends. The simple theory of BABYKIN et al. (1964) assumes zero temperature for the electrons and predicts that, for the conditions of our experiment, $n_s/n_2 \sim 10^{-3}$ would be sufficient to give stability, but if the effect of finite electron temperature is considered it appears that $n_s/n_2 \sim 1$ would be a more likely criterion*. In either case, it seems that the presence of slow plasma is an adequate reason for the observed stability in our experiment.

High frequency noise at about the ion cyclotron frequency has been reported from the PHOENIX and OGRA experiments, and is attributed to electrostatic instabilities arising from the highly anisotropic velocity distributions of the trapped

---

* R.J. Bickerton. Private communication.

ions in both these machines. No such noise was apparent on electrostatic probes in our experiment, probably because the instabilities were suppressed by the more isotropic velocity distribution produced by non-adiabatic trapping.

13. SUMMARY AND CONCLUSIONS

The resonant capture of 16 keV molecular hydrogen ions in a mirror trap has been shown to lead to a plasma of density $\sim 10^8$ cm^{-3} in a volume of 100 litres for an injection current of 40 mA: the system is thus comparable with other ion injection devices. The mean non-adiabatic lifetime of ions injected in a well-collimated beam corresponds to about 40 transits of the trap, but falls to about 18 transits when the angular divergence of the beam is increased. Protons formed inside the trap by dissociation of molecular ions on residual gas have a non-adiabatic lifetime of $\sim$ 700 transits.

No evidence of flute instability was found, although the density exceeded the theoretical threshold density by three orders of magnitude. This discrepancy is thought to be due to the stabilising effect of cold plasma which was present at a density of the same order as the fast ion density.

Single particle containment in the trap can be simulated by computation of particle orbits in a 'square-wave' model of the modulated field: the results obtained for the injected particles agree qualitatively and quantitatively with experiment. The observed containment of protons formed in the trap can be accounted for on the square-wave model if the effective modulation depth is reduced by a factor of 5 for these particles.

In the light of this study it is clear that the resonant trap is not a particularly efficient accumulator of particles. Its principal shortcoming is that only a small fraction of the available entry-exit paths are used for injection, while all are available for loss. To achieve the theoretical upper limit of accumulated density, as derived from Liouville's theorem, it is necessary to inject over all paths, and this can be achieved more efficiently in the stochastic

trap, with injection close to the edge of the loss cone. Re-arrangement of our apparatus to form a stochastic trap should theoretically lead to a 25-fold increase in density for the same beam current.

14. ACKNOWLEDGEMENTS

The authors wish to express their thanks to R.N. Hall, T.R. Pedley, K.R. Gamlen, B. Boardman and B.C. Sanders for their contributions to the engineering design of the apparatus and to J. Burt, M.F. Payne, P. Hedley, M.J. Terry, L. Barrow and R.F. Dyer for their assistance with the experiments. Discussions of the theory with Dr. E.W. Laing, and the assistance of Miss S.J. Roberts with the numerical calculations are also gratefully acknowledged.

15. REFERENCES

AFROSIMOV, V.V. et al. (1958) Zh. Eksp. Teor. Fiz., 34, 1398; Sov. Phys. JETP, 7, 968.

BABYKIN, M.V. et al. (1964) Zh. Eksp. Teor. Fiz., 47, 1631; Sov. Phys. JETP, 20, 1096.

BELL, P.R. et al. (1962) Nuclear Fusion, Suppl. Pt.1, 251.

DEMIRKHANOV, R.A. et al. (1964) Zh. Tekh. Fiz., 34, 60; Sov. Phys., Tech. Phys. 9, 45.

DREICER, H. et al. (1962) Nuclear Fusion, Suppl. Pt. 1, 299.

DUNNETT, D.A. et al. (1965) Plasma Physics (J. Nuclear Energy Part C) 7, 359.

FEDORCHENKO, V.D. et al. (1959) Zh. Tekh. Fiz., 29, 1212; Sov. Phys. Tech. Phys. 4, 1112.

GOLOVIN, I.N. et al. (1961) Usp. Fiz. Nauk. 73, 685; Sov. Phys., Uspekhi, 4, 323.

GOLOVIN, I.N. et al. (1964) Report IAE-676, I.V. Kurchatov Institute of Atomic Energy, Moscow. (CLM-Trans.6)

KADOMTSEV, B.B. (1961) Zh. Eksp. Teor. Fiz. 40, 328; Sov. Phys. JETP 13, 223.

KUO, L.G. et al. (1964) Phys. Fluids, 7, 988.

LAING, E.W. and ROBSON, A.E. (1961) Plasma Physics (J. Nuclear Energy Part C) 3, 146.

LLOYD, O. (1966) Brit. Journ. Appl. Phys. 17, 357.

McCLURE, G.W. (1963) Phys. Rev. 130, 1852.

READ, A.H. (1965) Brit. Journ. Appl. Phys. 16, 1861.

ROBSON, A.E. and TAYLOR, J.B. (1965) Phys. Fluids, 8, 2026.

SIMON, A. (1960) Plasma Physics (J. Nucl. Energy Part C) 1, 215.

SINELNIKOV, K.D. et al. (1960a) Zh. Tekh. Fiz. 30, 249; Sov. Phys. Tech. Phys. 5, 229.

SINELNIKOV, K.D. et al. (1960b) Zh. Tekh. Fiz. 30, 256; Sov. Phys. Tech. Phys. 5, 236.

WINGERSON, R.C. (1961) Phys. Rev. Letters 6, 446.

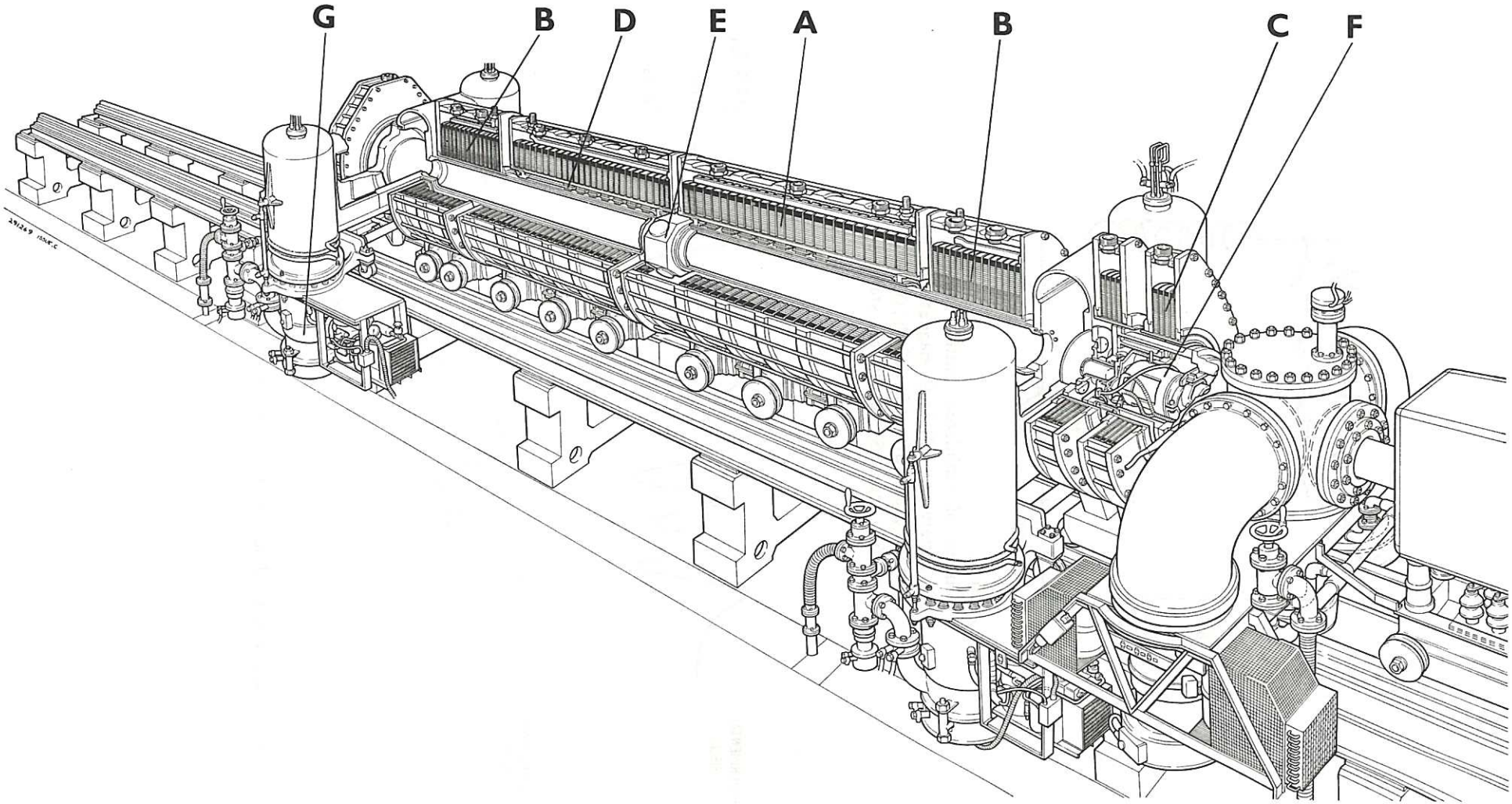

Fig. 1

(CLM-P 115)

General arrangement of resonant mirror trap. A - central field coil: B - mirror coil: C - injector coil: D - modulation coil: E - diagnostic block: F - ion source: G - diffusion pump

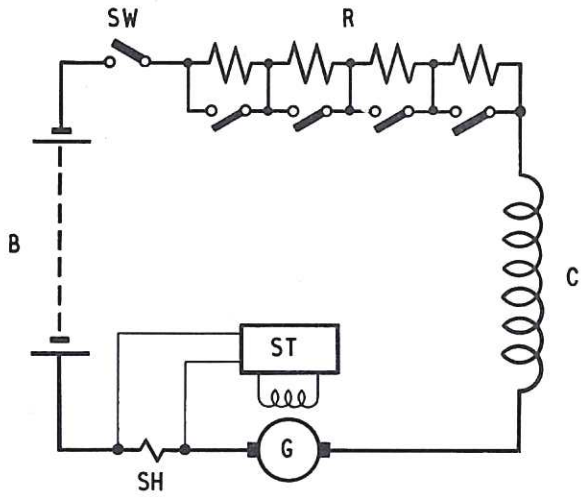

Fig. 2 (CLM-P115)
Circuit of stabilized battery supplies B - battery (360 cells) ; C - magnet coil ; R - resistor chain ; SW - main switch ; G - generator ; SH - shunt ; ST - electronic stabilizer

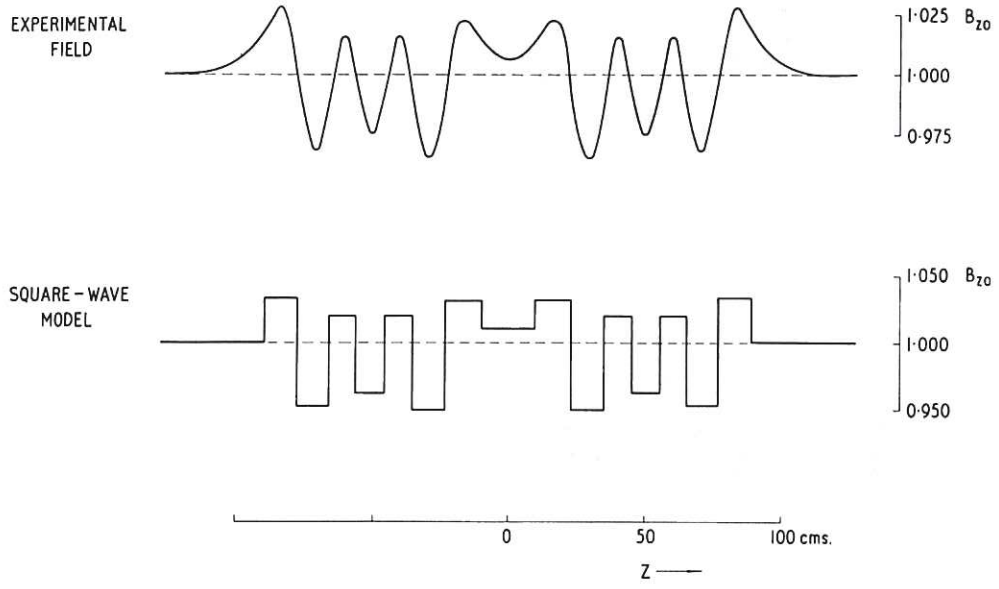

Fig. 3 Measured field on axis (B_z) and square wave model (CLM-P115)

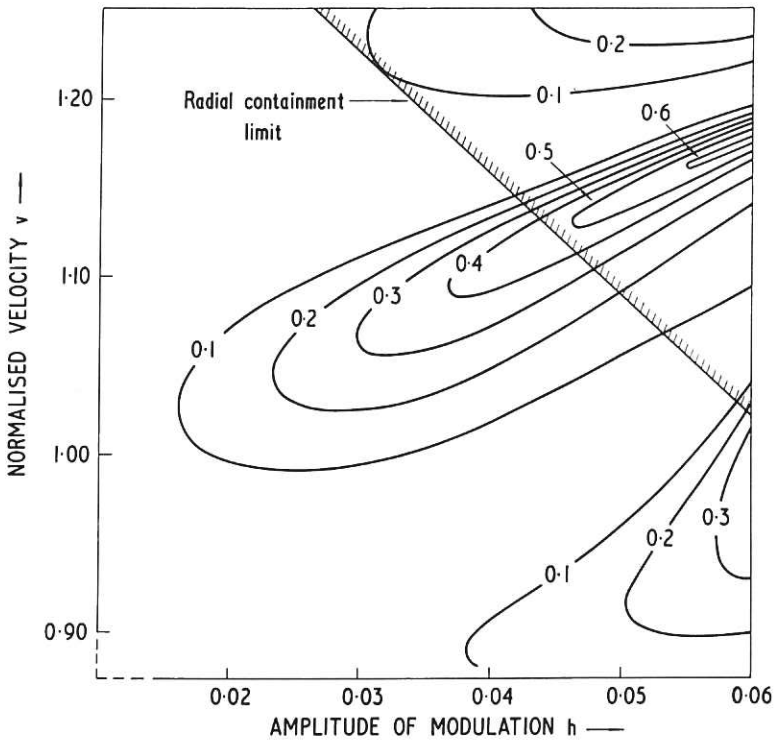

Fig. 4 (CLM-P 115)
Contours of ξ_1 as a function of h and v, first transit

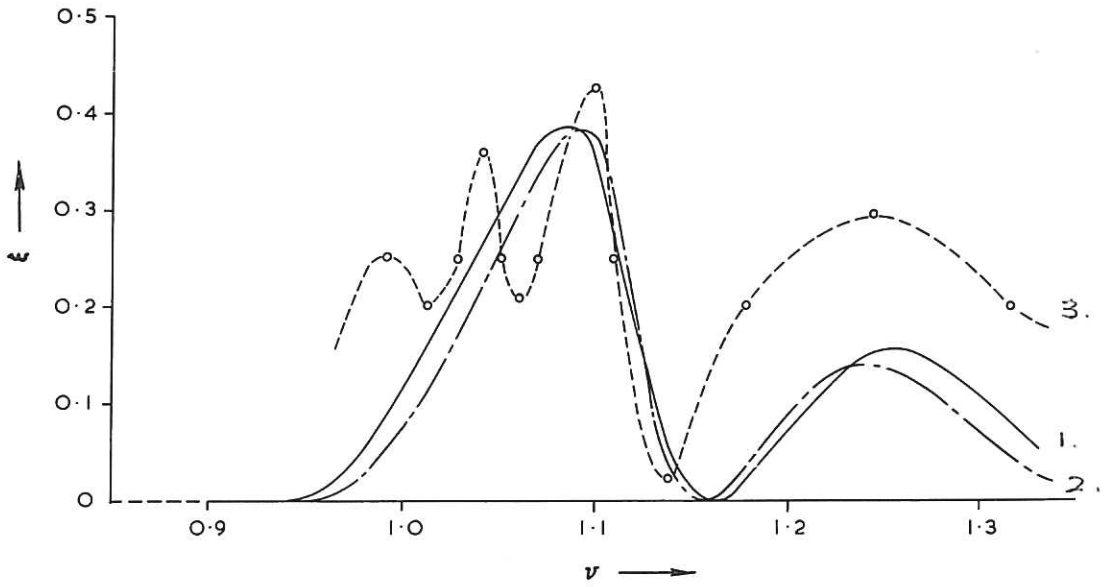

Fig. 5 (CLM-P 115)
ξ_1 as a function of v, first transit, h = 0.036. 1. orbits computed in real field, 2. orbits computed on square wave model, 3. electron experiment

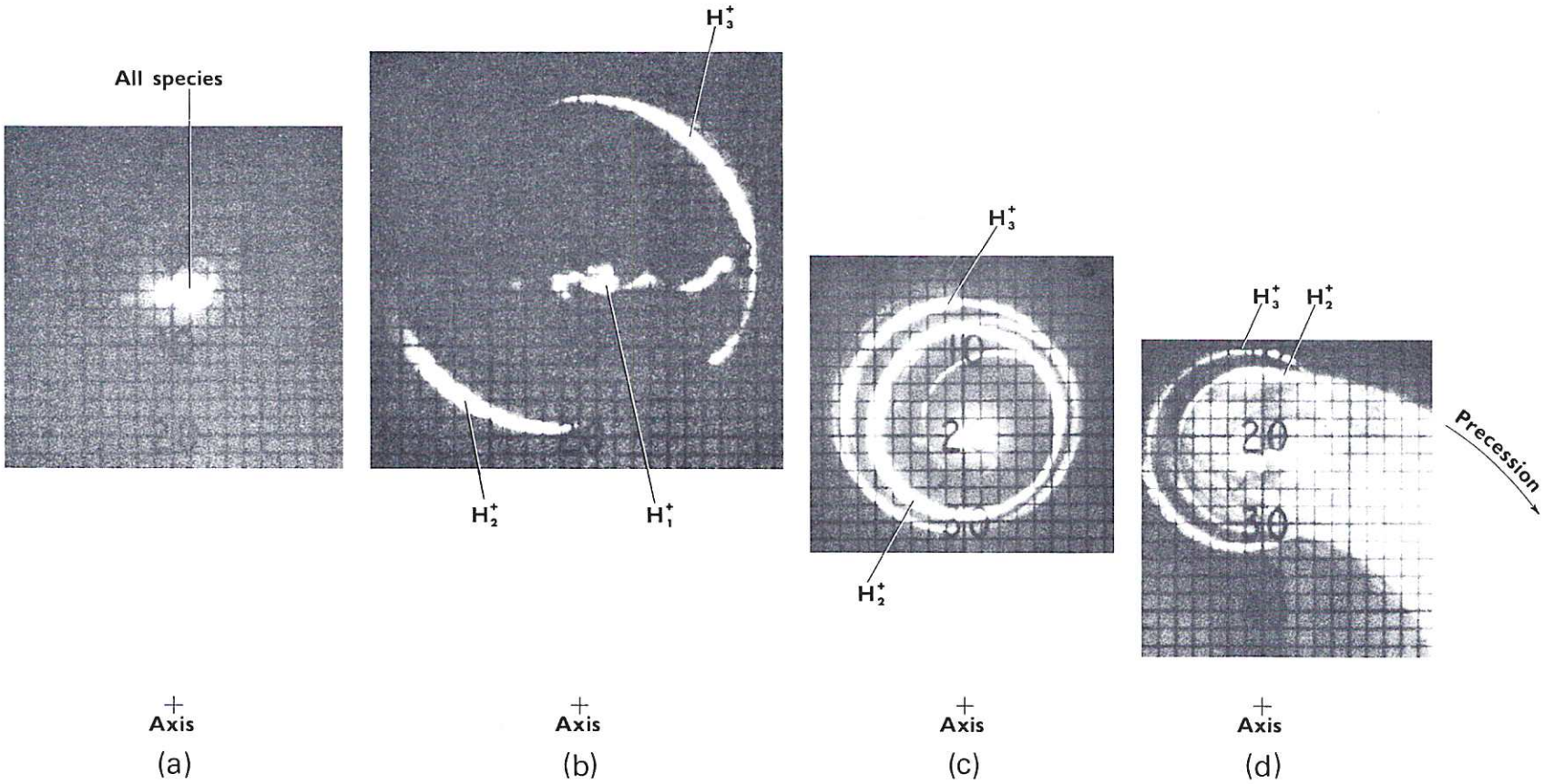

Fig. 6 (CLM-P 115)

Fluorescent screen patterns with ion injection. Field 7 kG, mirror ratio 4. Ion energy 14 kV ($v = 1.1$). Depth of modulation $h = 0.036$. (a) Screen 95 cm from midplane, modulation off. (b) As (a) but with modulation on. (c) Screen 125 cm from midplane. (d) Screen 135 cm from midplane.

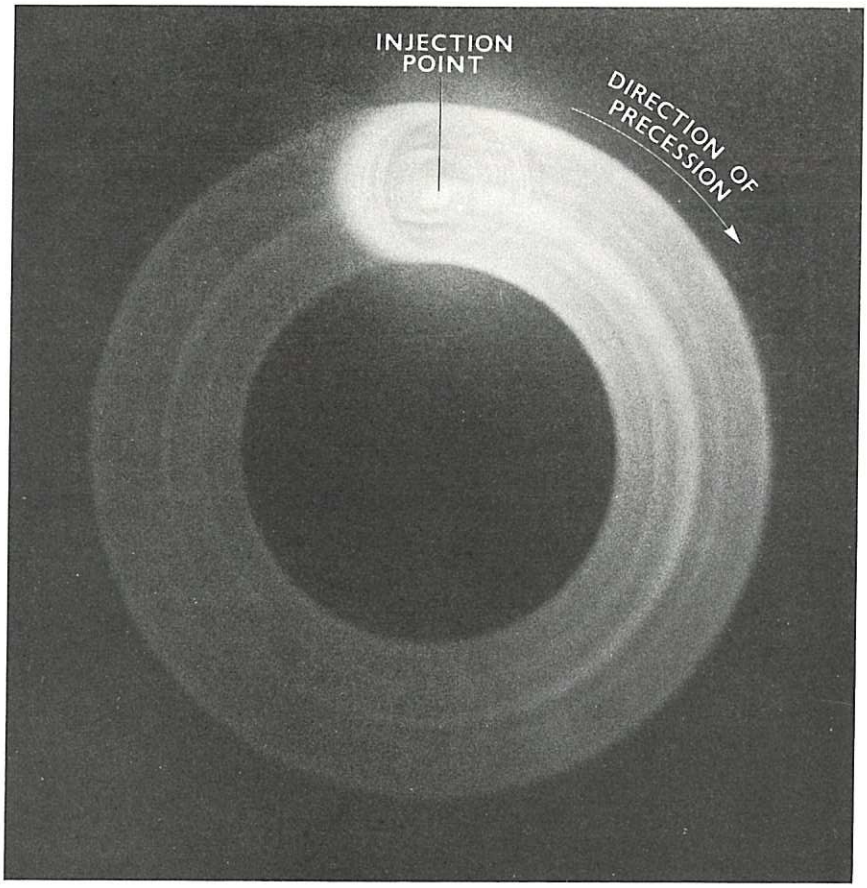

Fig. 7 (CLM-P 115)
Fluorescent screen pattern with electron injection.
Mirror ratio 4. v = 1.1, h = 0.036.

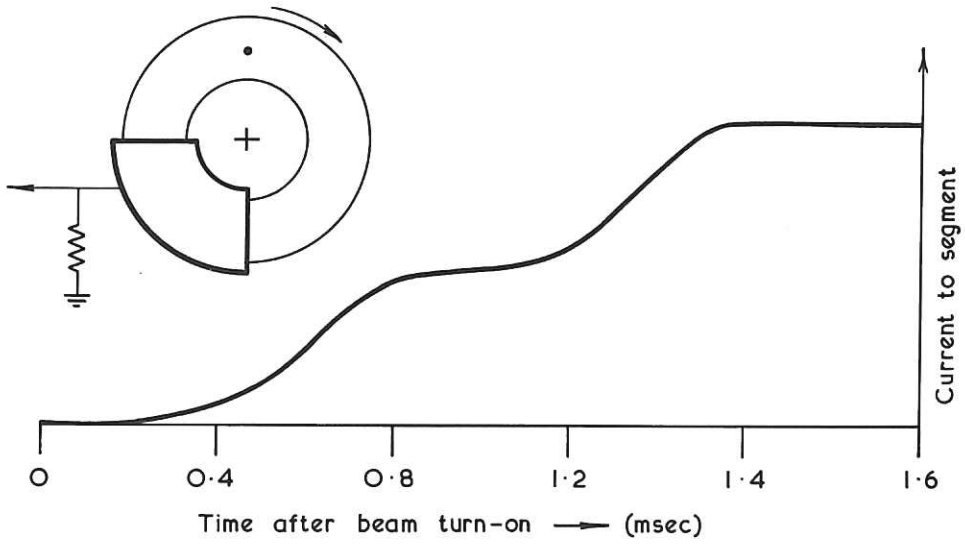

Fig. 8 (CLM-P 115)
Current to quadrant after turn-on of H_2^+ beam.
Inset: position of quadrant with respect to Fig. 7

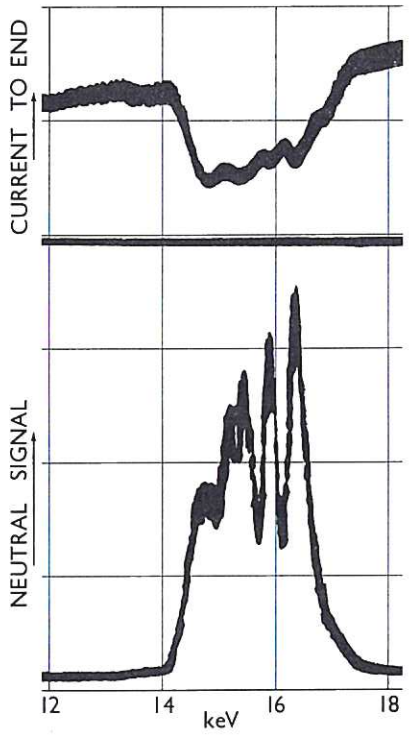

Fig. 9 (CLM-P 115)
Current to far end of machine and neutral particle signal as functions of ion energy. Field 7350 gauss, mirror ratio 4, h = 0.038. Collimator 1.

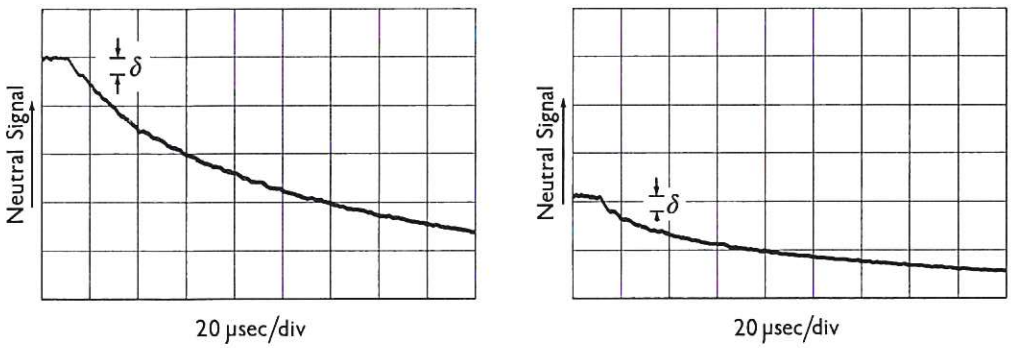

Fig. 10 (CLM-P 115)
Neutral signal decay curves after beam cut-off.
Field 7350 gauss, mirror ratio 4, h = 0.038.
(a) ion energy 16.4 kV (b) ion energy 15.6 kV

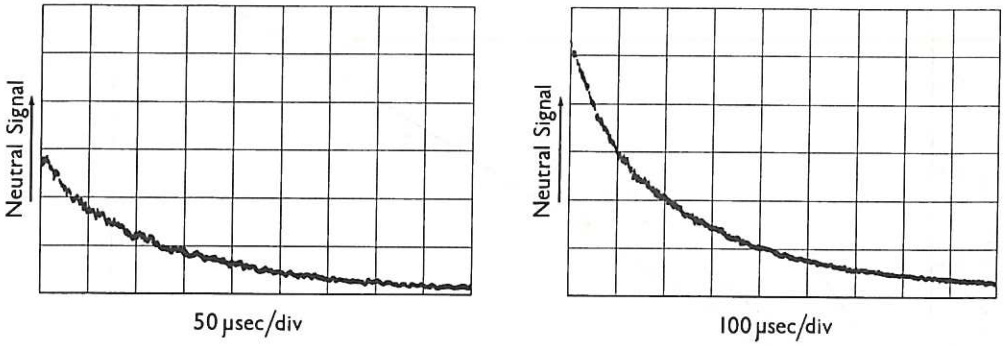

Fig. 11 (CLM-P 115)
Neutral signal decay curves (a) injection of 32.8 keV H_1^+; (b) injection of 16.4 keV H_2^+

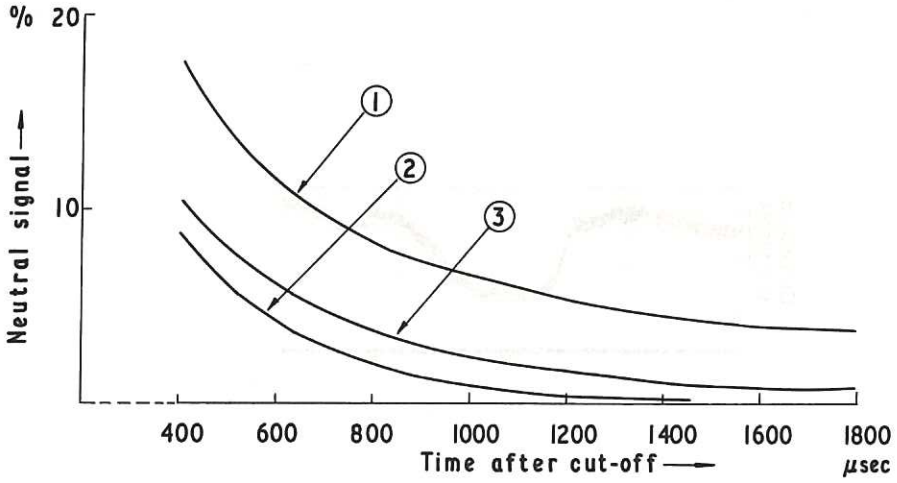

Fig. 12 (CLM-P 115)
Tails of H_2^+ decay curves. 1. Computed, $t_p = \infty$
2. Computed, $t_p = 0$; 3. Experimental ($t_p = 1400\,\mu$sec)

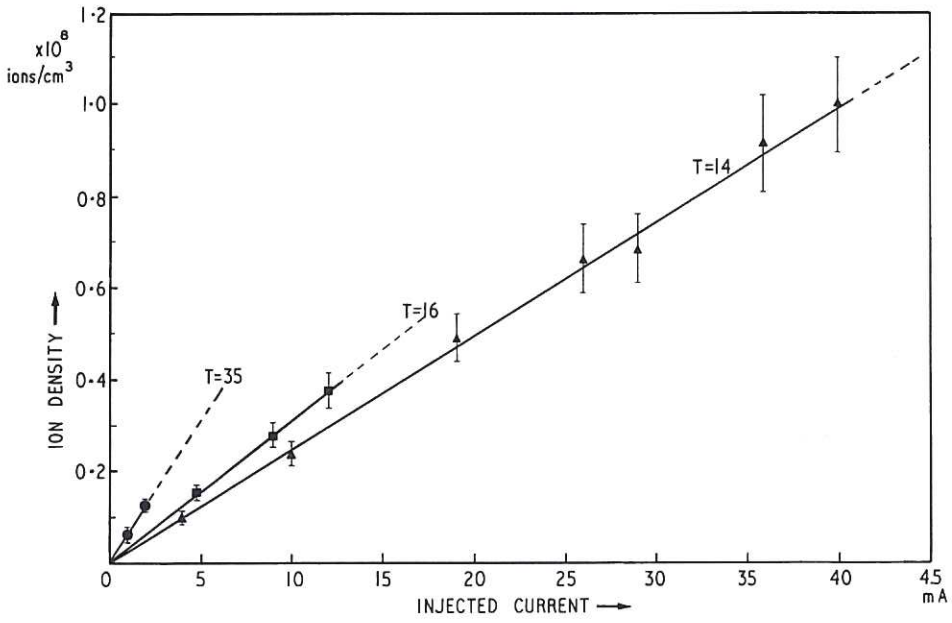

Fig. 13 (CLM-P 115)
Ion density as a function of injected current
Collimator 1 Collimator 2 Collimator 3

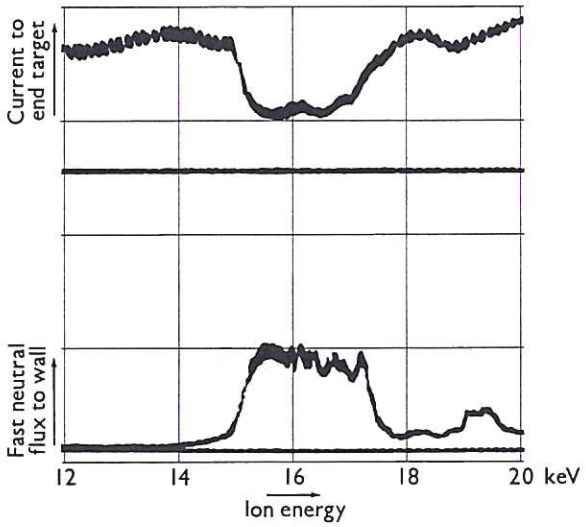

Fig. 14 (CLM-P 115)
Current to far end of machine and neutral particle signal as functions of ion energy. Conditions as Fig. 9, but with Collimator 2

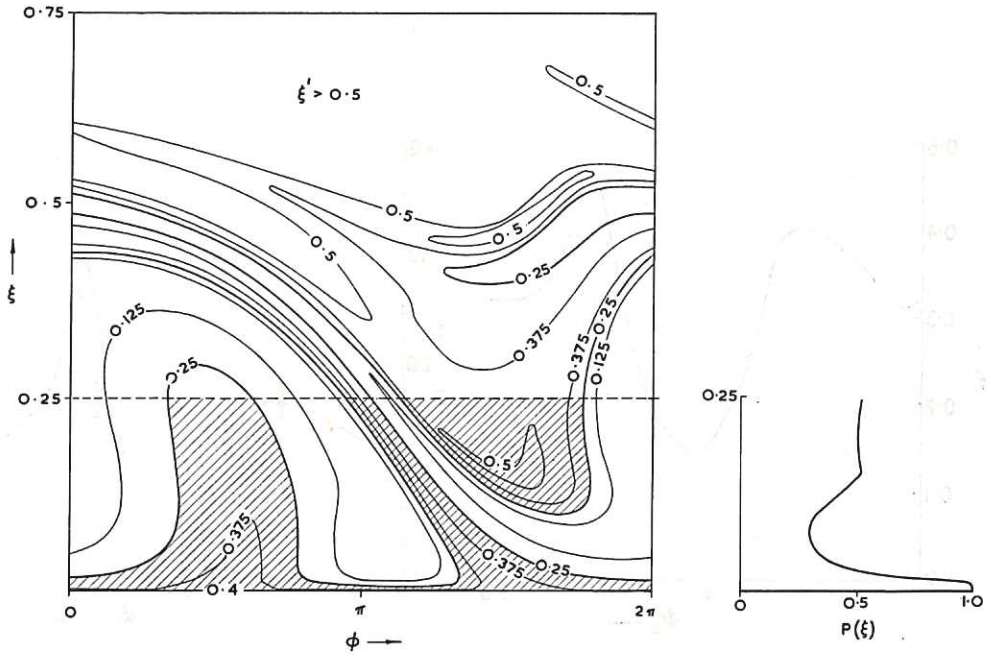

Fig. 15 (CLM-P 115)
(a) Contours of $\xi'(\xi, \phi)$ for $v = 1.1$, $h = 0.037$, from square wave model. (b) Capture probability $P(\xi)$

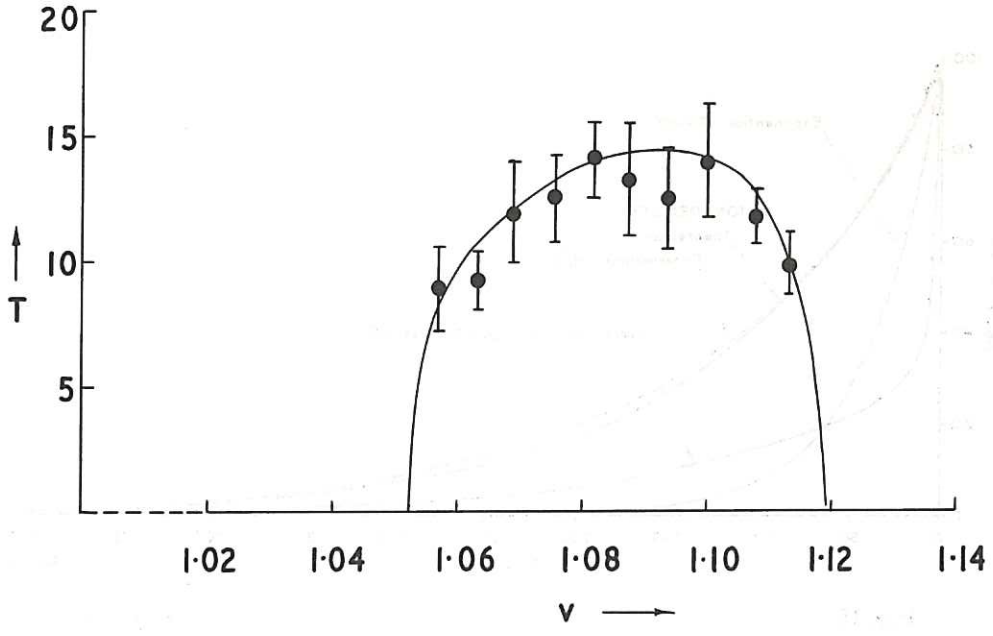

Fig. 16 (CLM-P 115)
Computed resonance curve, T as a function of v, $h = 0.037$. The error bars are derived from the statistics of the calculation

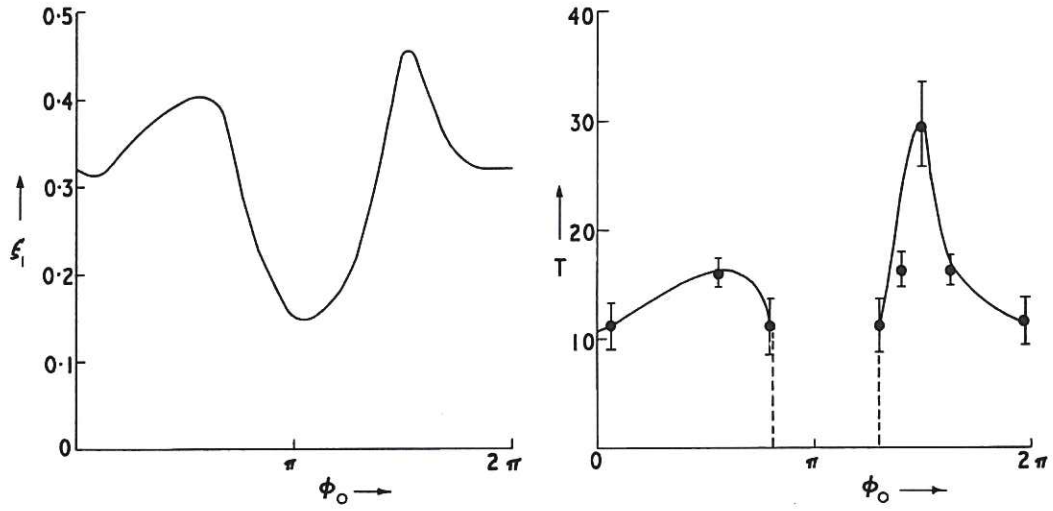

Fig. 17 (CLM-P 115)
(a) ξ_1' as a function of ϕ_0 for $\xi_0 = 0.01$ (from Fig. 15(a)) :
(b) T as a function of ϕ_0

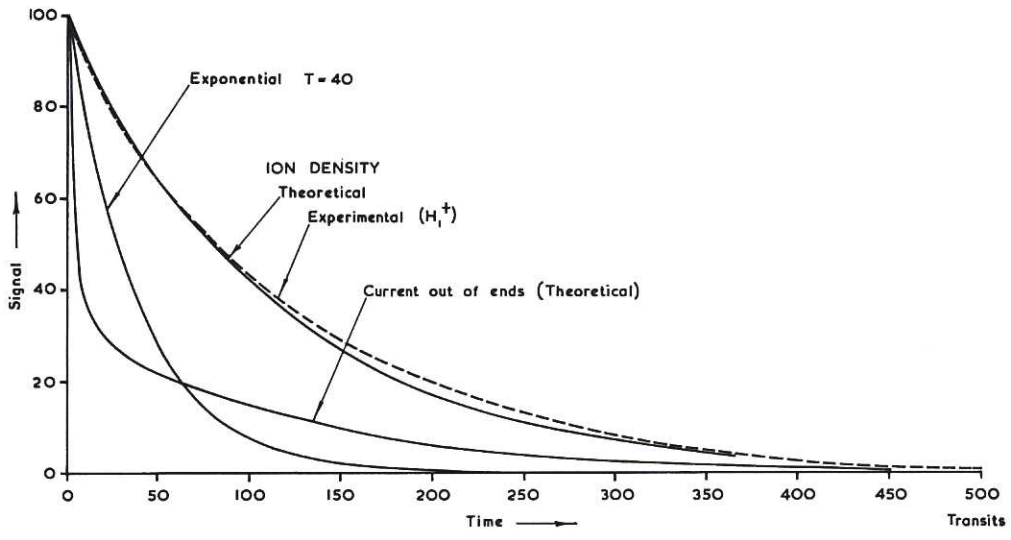

Fig. 18 (CLM-P 115)
Decay curves derived from square wave model compared with experimental curve (H_1^+) and exponential with same mean lifetime (T = 40)